



A continuous-time walking pattern generator for realizing seamless transition between flat-contact and heel-to-toe walking

Tazaki, Yuichi ; Hanasaki, Satomi ; Yukizaki, Soh ; Mitazono, Yugo ; Nagano, Hikaru ; Yokokohji, Yasuyoshi

(Citation)

Advanced Robotics, 37(5):316-328

(Issue Date)

2023-03-04

(Resource Type)

journal article

(Version)

Version of Record

(Rights)

© 2022 The Author(s). Published by Informa UK Limited, trading as Taylor & Francis Group

This is an Open Access article distributed under the terms of the Creative Commons Attribution-NonCommercial-NoDerivatives License...

(URL)

<https://hdl.handle.net/20.500.14094/0100477521>





A continuous-time walking pattern generator for realizing seamless transition between flat-contact and heel-to-toe walking

Yuichi Tazaki, Satomi Hanasaki, Soh Yukizaki, Yugo Mitazono, Hikaru Nagano & Yasuyoshi Yokokohji

To cite this article: Yuichi Tazaki, Satomi Hanasaki, Soh Yukizaki, Yugo Mitazono, Hikaru Nagano & Yasuyoshi Yokokohji (2022): A continuous-time walking pattern generator for realizing seamless transition between flat-contact and heel-to-toe walking, Advanced Robotics, DOI: [10.1080/01691864.2022.2120774](https://doi.org/10.1080/01691864.2022.2120774)

To link to this article: <https://doi.org/10.1080/01691864.2022.2120774>



© 2022 The Author(s). Published by Informa UK Limited, trading as Taylor & Francis Group



[View supplementary material](#)



Published online: 21 Sep 2022.



[Submit your article to this journal](#)



Article views: 145



[View related articles](#)



[View Crossmark data](#)

A continuous-time walking pattern generator for realizing seamless transition between flat-contact and heel-to-toe walking

Yuichi Tazaki^a, Satomi Hanasaki^a, Soh Yukizaki^b, Yugo Mitazono^b, Hikaru Nagano^a and Yasuyoshi Yokokohji^a 

^aDepartment of Mechanical Engineering, Graduate School of Engineering, Kobe University, Kobe, Japan; ^bKawasaki Heavy Industries, Ltd., Kobe, Japan

ABSTRACT

A planning algorithm that can generate continuous-time walking patterns including the seamless transition between flat-contact and heel-to-toe walking gaits is proposed. The planner makes use of the closed-form solution of a modified linear inverted pendulum mode which includes the ZMP and the weight ratio of each foot explicitly in its dynamics. The heel-to-toe movement of each foot is directly parameterized by the ZMP, and therefore consistency between the foot movement and the low-dimensional dynamics is ensured. In simulations with a 32 DoF model of a life-sized humanoid robot, fast human-like walking at the maximum speed of 4.6 km/h was achieved.

ARTICLE HISTORY

Received 25 April 2022
Revised 24 July 2022
Accepted 31 July 2022

KEYWORDS

Humanoid robot; motion planning; walking pattern generation; human-like walking

1. Introduction

1.1. Need for humanoid robots with better mobility

Humanoid robots are expected to assist humans in daily lives as well as to perform labor in their stead. In order for a humanoid robot to work efficiently without being an obstruction to humans, its level of mobility should match or at least be close to that of humans. Conventional bipedal walking robots walk with flat-contact between the feet and the ground. Assuming flat-contact simplifies walking pattern generation since the feet can be kept level with the ground during walking. It also simplifies balance control, because the support region, which determines the feasible region of the ZMP, is unchanged while each foot is in contact with the ground. However, flat-contact walking does not allow fast walking with a long stride. Moreover, the center-of-mass must be held low in order to avoid kinematic singularity, and this results in a high load on the knee joints and a robot-like appearance of walking. Some modern bipedal and humanoid robots that achieved fast walking overcame these shortcomings by utilizing human-like walking involving toe-off, heel-strike, and knee stretching [1,2]. One exception would be the bipedal robot Cassie [3], which recently achieved 5 km/h walking with bird-like leg design. In this case, however, high cadence (roughly 0.3 s per step) largely contributed to high walking speed, which requires a light-weight leg design. For humanoid robots with relatively

large leg inertia, simulating a human-like walking gait and thereby increasing the step length is considered to be a more effective strategy to achieve high walking speed. It was also reported in studies on bipedal running that toe-off and heel-strike could effectively increase step length and reduce landing impact [4,5].

1.2. Review of walking pattern generation methods for fast and human-like walking

To date, various methods for realizing human-like fast walking have been proposed in the literature [2,6–14]. Bipedal walking involving toe-off and heel-strike (heel-to-toe walking for short) poses a number of technical challenges compared to conventional flat-contact walking.

The first issue is how to mathematically represent the movement of the ZMP. As the contact state changes from heel-contact to mid-stance and then to toe-contact, the ZMP must also move between respective contact regions. Various representations of the ZMP trajectory discussed in the literature include: discontinuous trajectory that moves through a series of fixed points [12], piecewise exponential trajectory [7], cubic spline [2], and piecewise linear trajectory ([8,10] and [11]).

The second issue is how to ensure consistency between kinematics and dynamics. In Ref. [13], the movement of the feet and the waist was designed first in consideration

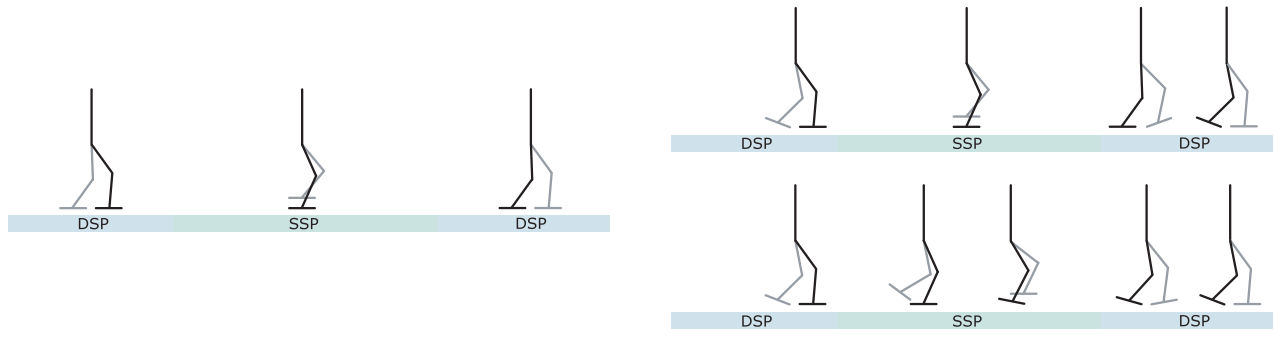


Figure 1. Half walking cycle of different walking gaits. Flat-contact (left), heel-to-toe with heel-off during DSP (top right), and heel-to-toe with heel-off during SSP (bottom right).

with kinematic limits, and the trajectories of the CoM and the ZMP were generated by using the preview control [15]. In Ref. [2], the ZMP trajectory and the movement of the feet were designed separately, and their inconsistency was minimized by applying a dynamics filter in the later stage. In either case, since they design kinematic and dynamic movements in a separate manner, their consistency is not completely ensured. In Ref. [14], a prioritized inverse kinematics (IK) solver was used for generating whole-body motion respecting kinematic limits and a ZMP-based stability criterion. As a result, heel-off movement was naturally realized without explicitly specifying reference trajectories of the feet. It was reported, however, that kinematic singularity and change of contact state caused abrupt change of velocity.

The third issue is how to systematically determine the order of contact state transition. As pointed out in [16], heel-to-toe walking gait has a number of minor types including ones illustrated in Figure 1. In the type shown in the upper right of the figure, the heel-strike of the swing foot occurs before the heel of the support foot lifts off the ground, while in the one shown in the lower right, the order is the opposite. The former type is more desirable in terms of stability because contact transition occurs during the double support phase, while its maximum allowable step length is limited. The latter type, on the other hand, can achieve greater step length but it poses a greater risk of instability because heel-off occurs during the single support phase. In addition, one can consider other minor types in which either heel-off or heel-strike does not occur. In most existing studies, only one of these minor types was focused on, and the order of contact transition was predefined. In practical situations, the robot must not only walk at a fixed speed but also walk at different speeds with appropriate acceleration and deceleration. The planner is therefore required to produce a walking pattern consisting of multiple different gaits according to every input sequence of various step length and step duration.

1.3. Contribution of this paper

The main contribution of this paper is to propose a method that can generate walking patterns consisting of flat-contact and heel-to-toe gaits depending on walking speed, acceleration and deceleration. The proposed planner requires only footsteps and step durations as inputs, and generates reference foot trajectories with heel-to-toe contact transition together with reference trajectories of the CoM and the ZMP that are dynamically consistent with the foot movement. The main idea is to express the trajectory of the ZMP and the weight ratio of each foot explicitly in the model. This is a major difference from existing methods, which only considered the overall ZMP (that is, the weighted average of the ZMPs of the feet). The heel-to-toe movement of each foot is parameterized by the relative position of the ZMP of that foot and the curved profile of the sole. In this manner, various walking modes including flat-contact and heel-to-toe can be generated without predefined contact transition sequences. Moreover, unlike [2], no a posteriori dynamics filtering is required because the consistency of kinematics and dynamics is ensured by definition. A closed-form solution of the linear inverted pendulum mode (LIPM) with time-varying ZMP and weight ratio is derived and used for walking pattern generation. Planned trajectory is segmented solely based on walking phases. In this manner, continuous-time trajectories of the CoM can be planned with a small number of decision variables compared to conventional methods based on time-discretization with a fixed sampling period. The proposed walking pattern generator is evaluated in dynamical simulation using a 32-DoF model of a life-sized humanoid robot, in which the maximum walking speed of 4.6 km/h was achieved.

2. Low-dimensional dynamical model of center-of-mass movement

Under the assumption that the angular momentum around the CoM is constant, the movement of the CoM is

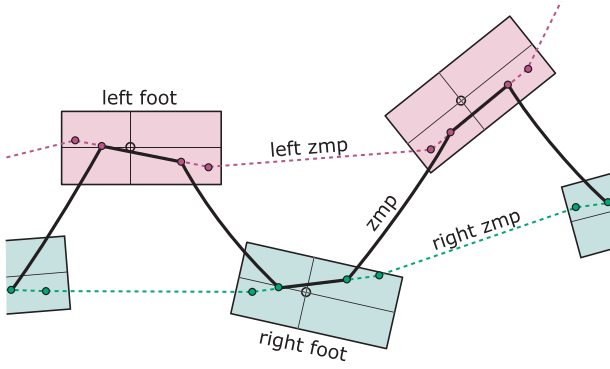


Figure 2. Relationship of footsteps and ZMP.

governed by the linear inverted pendulum mode (LIPM), which can be written as follows.

$$\ddot{\mathbf{p}}_{\text{com}}(t) = \frac{1}{T^2}(\mathbf{p}_{\text{com}}(t) - \mathbf{p}_{\text{zmp}}(t)) - \mathbf{g} \quad (1)$$

The 3D LIPM shown above has been used in recent studies such as [17], while the original 2D LIPM and early attempt to extend it to 3D can be found in [15]. Here, $\mathbf{p}_{\text{com}} \in \mathbb{R}^3$ and $\mathbf{p}_{\text{zmp}} \in \mathbb{R}^3$ are the position of the CoM and the ZMP in 3D space, respectively, $\mathbf{g} = [0 \ 0 \ g]^T$ is the acceleration of gravity, and $T > 0$ is an arbitrary positive constant. In a simple setting of walking on a level ground with the height (the z coordinate) of the CoM fixed to a constant h , T is set as $\sqrt{\frac{h}{g}}$, and the z coordinate of the CoM and ZMP are fixed to h and 0, respectively. We assume this simple setup henceforth.

Figure 2 illustrates the relationship between footsteps, the ZMP, and the ZMP of each foot. Here, the ZMP of each foot is simply defined as the center-of-pressure of contact force distribution applied to that foot. It is essential to express the ZMP of each foot explicitly in our formulation because this information is directly utilized for generating heel-to-toe movement in the later stage. Consider a certain time interval $[t_k, t_{k+1}]$ where $t_{k+1} = t_k + \tau_k$. Let us assume that the ZMP of each foot moves with a constant velocity during this period:

$$\mathbf{p}_{\text{zmp},i}(t) = \mathbf{p}_{\text{zmp},i,k} + \mathbf{v}_{\text{zmp},i,k}(t - t_k). \quad (2)$$

where i is the foot label which takes r indicating the right foot or l indicating the left. The ZMP (in the ordinary sense) can be expressed as a weighted average of the ZMPs of the two feet:

$$\mathbf{p}_{\text{zmp}}(t) = w_r(t)\mathbf{p}_{\text{zmp},r}(t) + w_l(t)\mathbf{p}_{\text{zmp},l}(t). \quad (3)$$

Here, $w_i(t) \in [0, 1]$ ($i \in \{r, l\}$) is the weight ratio of each foot, where $w_r + w_l = 1$ always holds. We also assume that the weight ratio of each foot changes linearly during

$[t_k, t_{k+1}]$:

$$w_i(t) = \left(1 - \frac{t - t_k}{\tau_k}\right) w_{i,k} + \left(\frac{t - t_k}{\tau_k}\right) w_{i,k+1} \quad (4)$$

By substituting (2) and (4) to (3), we obtain

$$\begin{aligned} \mathbf{p}_{\text{zmp}}(t) &= \mathbf{p}_{\text{zmp},k} + \mathbf{v}_{\text{zmp},k}(t - t_k) + \frac{1}{2}\mathbf{a}_{\text{zmp},k}(t - t_k)^2, \\ \mathbf{p}_{\text{zmp},k} &= \sum_i w_{i,k}\mathbf{p}_{\text{zmp},i,k}, \\ \mathbf{v}_{\text{zmp},k} &= \sum_i w_{i,k}\mathbf{v}_{\text{zmp},i,k} + \frac{1}{\tau_k}(w_{i,k+1} - w_{i,k})\mathbf{p}_{\text{zmp},i,k}, \\ \mathbf{a}_{\text{zmp},k} &= \sum_i \frac{2}{\tau_k}(w_{i,k+1} - w_{i,k})\mathbf{v}_{\text{zmp},i,k} \end{aligned} \quad (5)$$

Thus the movement of the ZMP is generally expressed as a quadratic function of time.

By substituting (5) into (1) and solving the ODE, one can derive the closed-form solution for the position of the CoM as shown below.

$$\begin{aligned} \mathbf{p}_{\text{com}}(t) &= \mathbf{p}_{\text{zmp},k} + (\mathbf{a}_{\text{zmp},k} + \mathbf{g})T^2 + \mathbf{v}_{\text{zmp},k}(t - t_k) \\ &\quad + \frac{1}{2}\mathbf{a}_{\text{zmp},k}(t - t_k)^2 \\ &\quad + (\mathbf{p}_{\text{com},k} - (\mathbf{p}_{\text{zmp},k} + (\mathbf{a}_{\text{zmp},k} + \mathbf{g})T^2)) \\ &\quad \cosh\left(\frac{t - t_k}{T}\right) \\ &\quad + T(\mathbf{v}_{\text{com},k} - \mathbf{v}_{\text{zmp},k})\sinh\left(\frac{t - t_k}{T}\right) \end{aligned} \quad (6)$$

The velocity of the CoM can also be obtained in the closed form by differentiating (6).

3. Bipedal walking trajectory generation considering heel-to-toe contact

3.1. Overview

The proposed walking pattern generator consists of two stages. The first stage accepts footsteps and step durations as inputs. These information should be either specified manually or generated by an external footstep planner. Based on these inputs, in the first stage, the planner automatically generates trajectories of the CoM and the ZMP of each foot. In the second stage, the planner generates a continuous trajectory of each foot based on the trajectory of the ZMP passed from the first stage. Since walking pattern generation for several walking steps requires computation time in the order of seconds, it is performed offline;

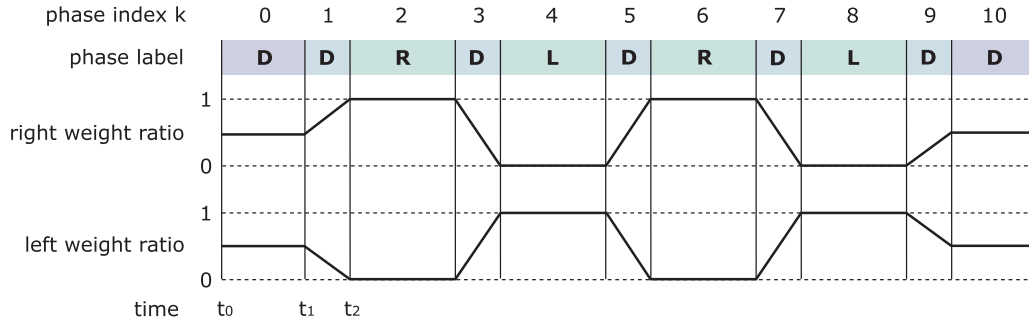


Figure 3. Illustration of walking phase and related symbols.

that is, outside of the real-time control loop. In the real-time control loop, the desired angle and angular velocity of each joint is computed by means of inverse kinematics from the desired trajectory generated by the planner. Moreover, the desired ZMP is converted to desired contact wrench and provided to the ground reaction force controller. Another major benefit of the proposed planner is that, since it outputs the desired ZMP and weight ratio of each foot explicitly, calculating the equivalent contact wrench is straightforward, even for double support phases. In the case of conventional planners, desired contact wrench of each foot together with the appropriate weight ratio must be determined at this stage, and it is hard to ensure the existence of valid contact wrench, especially for double support phases involving heel-to-toe contact transition. Further detail of our implementation of the real-time control loop is omitted due to the limitation of space.

3.2. CoM and ZMP trajectory generation

Let us consider a time interval $[0, t_f]$. This interval is divided into N phases, where the time interval of the k -th phase is expressed as $[t_k, t_k + \tau_k]$ with $t_0 = 0$. The contact state of each foot, that is, whether each foot is in contact with the ground or not, is invariant during each phase. Each phase is assigned one of the following labels depending on its contact state: R (right support), L (left support), and D (double support). Moreover, $s_{i,k}$ denotes the step count of the foot i ($i \in \{r, l\}$) during the k -th phase; namely, $s_{i,k}$ starts from 0 and is incremented each time the foot i changes its foothold. See Figure 3 for the relationship of these symbols. As shown in the figure, extra D phases are inserted at the beginning and the end of the sequence. These D phases are assigned greater duration than other D phases inserted between R and L phases. This is to ensure sufficient time for accelerating and decelerating the CoM at the beginning and the end of walking, respectively. The weight ratio of each foot is determined solely based on contact states, as illustrated

in the figure. Namely, during each single support phase (SSP), the weight ratio of the support foot is fixed to 1, while that of the swing foot is fixed to 0. During the first and the last double support phase (DSP), the weight ratio of both feet is fixed to 0.5. During other intermediate DSPs, the weight ratio changes linearly.

The planning problem of the CoM and ZMP trajectories is formulated as a constrained optimal control problem. Let us define the state variable and the input variable as

$$\mathbf{x}_k = \begin{bmatrix} \mathbf{p}_{\text{com},k} \\ \mathbf{v}_{\text{com},k} \\ \mathbf{p}_{\text{zmp},r,k} \\ \mathbf{p}_{\text{zmp},l,k} \end{bmatrix} \in \mathbb{R}^{12}, \quad \mathbf{u}_k = \begin{bmatrix} \mathbf{v}_{\text{zmp},r,k} \\ \mathbf{v}_{\text{zmp},l,k} \end{bmatrix} \in \mathbb{R}^6 \quad (7)$$

From (2) and (6), the update law of the state variable from t_k to t_{k+1} is derived as follows.

$$\begin{aligned} \mathbf{p}_{\text{com},k+1} &= \mathbf{p}_{\text{zmp},k} + (\mathbf{a}_{\text{zmp},k} + \mathbf{g})T^2 + \mathbf{v}_{\text{zmp},k}\tau_k \\ &\quad + \frac{1}{2}\mathbf{a}_{\text{zmp},k}\tau_k^2 \\ &\quad + (\mathbf{p}_{\text{com},k} - (\mathbf{p}_{\text{zmp},k} + (\mathbf{a}_{\text{zmp},k} + \mathbf{g})T^2)) \\ &\quad \cosh\left(\frac{\tau_k}{T}\right) + T(\mathbf{v}_{\text{com},k} - \mathbf{v}_{\text{zmp},k})\sinh\left(\frac{\tau_k}{T}\right) \end{aligned} \quad (8)$$

$$\begin{aligned} \mathbf{v}_{\text{com},k+1} &= \mathbf{v}_{\text{zmp},k} + \mathbf{a}_{\text{zmp},k}\tau_k \\ &\quad + \frac{1}{T}(\mathbf{p}_{\text{com},k} - (\mathbf{p}_{\text{zmp},k} + (\mathbf{a}_{\text{zmp},k} + \mathbf{g})T^2)) \\ &\quad \sinh\left(\frac{\tau_k}{T}\right) + (\mathbf{v}_{\text{com},k} - \mathbf{v}_{\text{zmp},k})\cosh\left(\frac{\tau_k}{T}\right) \end{aligned} \quad (9)$$

$$\begin{aligned} \mathbf{p}_{\text{zmp},i,k+1} &= \mathbf{p}_{\text{zmp},i,k} + \mathbf{v}_{\text{zmp},i,k}\tau_k \quad (i \in \{r, l\}) \end{aligned} \quad (10)$$

From these equations, we can define the state equation $\mathbf{x}_{k+1} = f(\mathbf{x}_k, \mathbf{u}_k)$.

Moreover, the ZMP of each foot must be inside the support polygon. This constraint is expressed as follows.

$$\underline{\mathbf{p}}_{\text{zmp},i,s} \leq R_{\text{foot},i,s}^T (\mathbf{p}_{\text{zmp},i,k} - \mathbf{p}_{\text{foot},i,s}) \leq \bar{\mathbf{p}}_{\text{zmp},i,s} \quad (i \in \{r, l\}), s = s_{i,k} \quad (11)$$

Here, $\mathbf{p}_{\text{foot},i,s}$ and $R_{\text{foot},i,s}$ are the position and the orientation of the s -th foothold of the foot i . Moreover, $\underline{\mathbf{p}}_{\text{zmp},i,s}$ and $\bar{\mathbf{p}}_{\text{zmp},i,s}$ define lower and upper bound on the ZMP. The inequalities are evaluated componentwise.

We consider the following quadratic cost function to be minimized:

$$J = \frac{1}{2} \left[\sum_{k=1}^{N-1} \epsilon^2 \|\mathbf{v}_{\text{com},k}\|^2 + \|\mathbf{p}_{\text{com},N} - \mathbf{p}_{\text{com},f}\|^2 + \|\mathbf{v}_{\text{com},N}\|^2 \right] \quad (12)$$

The terminal costs are set to ensure that the CoM comes to a halt at the desired position at the terminal time. The stage costs are set to penalize excessive CoM velocity in the meantime. Here, ϵ is given a small value to assign lower priority to the stage cost compared to the terminal cost.

The trajectory planning problem is expressed as the following optimal control problem:

$$\begin{aligned} & \text{minimize } J \\ & \text{subject to } \mathbf{x}_{k+1} = f(\mathbf{x}_k, \mathbf{u}_k) \quad \forall k = 0, 1, \dots, N-1 \\ & (11) \quad \forall k = 0, 1, \dots, N \end{aligned} \quad (13)$$

In this study, we view this problem as a single large-scale least-squares problem and solve it by using the Gauss–Newton method. Inequality constraints are treated as penalty functions and put into the cost function. Here, each penalty term is defined as a quadratic function of deviation of the decision variable from the constraint boundary. One disadvantage is that the computational complexity is $O(N^3)$ since we need to solve a linear system of equations of the size proportional to N . For generating long walking patterns, it would be better to apply optimal control methods such as differential dynamic programming (DDP), since their complexity is linear with respect to N .

3.3. Foot trajectory generation

In this section, a method to generate a support foot trajectory including heel-to-toe contact transition and a swing foot trajectory that smoothly connects toe-off and

heel-strike is described. To simplify the design flow, the overall movement is decomposed into two movements, one is the movement of the virtual *footbase* relative to the ground, and the other is the heel-to-toe movement of the foot relative to the footbase. Figure 4 illustrates the relationship between the ground, the footbase, and the foot. The xy plane of the footbase is always parallel to the ground. Therefore, the movement of the footbase is expressed by translation in three directions (x , y , and z) and rotation around the z -axis (i.e. yaw rotation). The relative movement of the foot with respect to the footbase is constrained on the xz plane of the footbase. Thus, its movement is expressed by translation in two directions (x and z) and rotation around the y -axis (i.e. pitch rotation). For simple notation, let us omit the subscript i in the following discussion. Let the position of the footbase in the global coordinate be $\mathbf{p}' \in \mathbb{R}^3$, and its rotation angle around the z -axis be $\theta \in \mathbb{R}$. Moreover, let the position of the foot in the x – z plane of the local coordinate frame of the footbase be $\mathbf{p}'' \in \mathbb{R}^2$ and its rotation angle around the y -axis be $\phi \in \mathbb{R}$. Then the global position and orientation of the foot are expressed as follows.

$$\mathbf{p} = \mathbf{p}' + R_z(\theta) \begin{bmatrix} 1 & 0 \\ 0 & 0 \\ 0 & 1 \end{bmatrix} \mathbf{p}'', \quad R = R_z(\theta) R_y(\phi) \quad (14)$$

Here, R is a rotation matrix expressing the orientation of the foot, and R_y and R_z express rotation around the y and z axis, respectively.

The footbase of the support foot matches the corresponding foothold and it makes no relative movement with respect to the ground. The footbase of the swing foot moves from the current foothold to the next one. In order to ensure the continuity of velocity, the linear and angular velocity at the beginning and the end of the swing phase must be zero. There are several possible choices for concrete parametrization satisfying these boundary conditions. One example is a parametrization based on cycloid as shown below.

$$\begin{aligned} \mathbf{p}'(t) = & \mathbf{p}_s + c_h \left(\frac{t - t_k}{\tau_k} \right) (\mathbf{p}_{s+1} - \mathbf{p}_s) \\ & + c_v \left(\frac{t - t_k}{\tau_k} \right) h_{\text{lift}}, \end{aligned} \quad (15)$$

$$\theta(t) = \theta_s + c_h \left(\frac{t - t_k}{\tau_k} \right) (\theta_{s+1} - \theta_s) \quad (16)$$

Here, \mathbf{p}_s and θ_s are the position and the yaw angle of the s -th foothold, respectively, and h_{lift} is a constant that specifies the maximum clearance from the ground. Moreover,

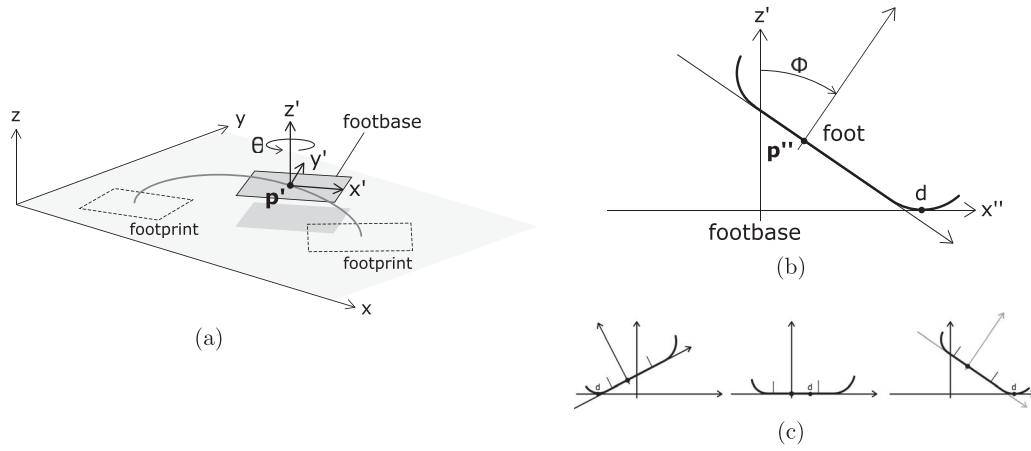


Figure 4. Relationship between the ground, the footbase, and the foot. (a) The ground and the footbase, (b) the footbase and the foot and (c) foot pitch movement.

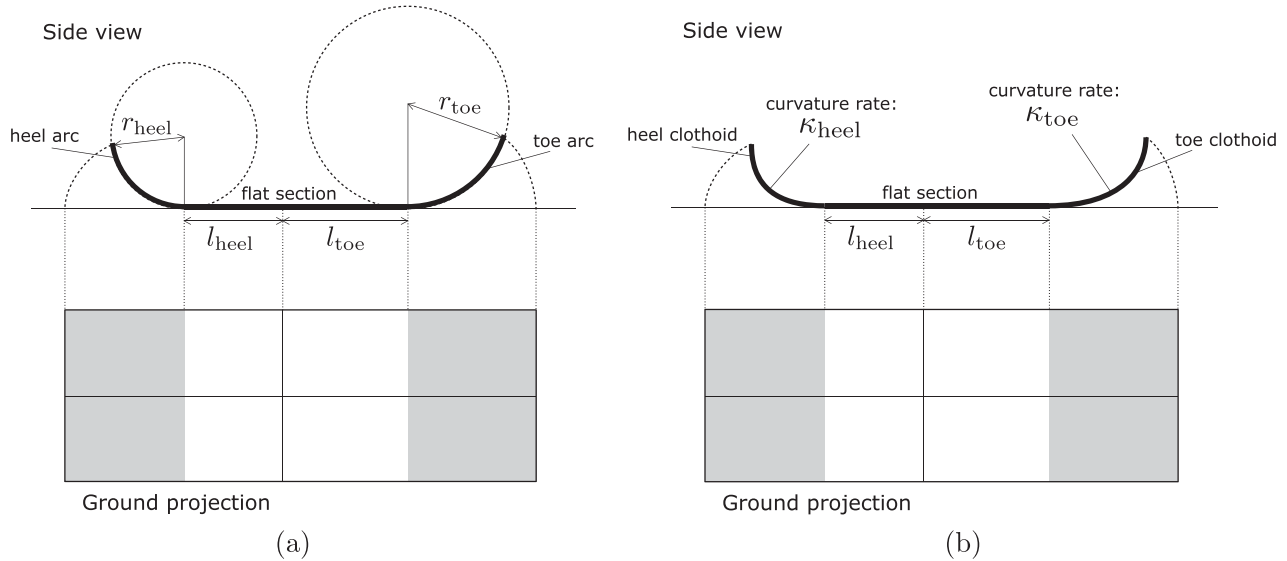


Figure 5. Foot shape with curved ends. (a) Circular arc (b) and clothoid.

$c_h(s)$ and $c_v(s)$ are cycloid functions defined as

$$c_h(s) = s - \frac{\sin(2\pi s)}{2\pi}, \quad c_v(s) = \frac{1 - \cos(2\pi s)}{2}$$

The relative movement of the foot with respect to the footbase is determined by the geometric shape of the sole and a scalar parameter d which is the position of a point at which the sole touches the x -axis of the footbase. As illustrated in Figure 5(a,b), we assume that the lower profile of the foot consists of a flat section in the middle and curved sections on both ends called the heel arc and the toe arc. Here, two types of curves are considered: *circular arc* and *clothoid arc*. The circular arc has a constant curvature (which is the inverse of the radius), whereas the clothoid arc has varying curvature which is zero at the boundary

between the flat section and linearly increases towards the end of the curved section. The circular arc is parameterized r_{heel} and r_{toe} , which are the curvature radius of the heel arc and the toe arc, respectively. The clothoid arc, on the other hand, is parametrized by κ_{heel} and κ_{toe} , which are the rate of change of curvature of the heel arc and the toe arc, respectively. As illustrated in Figure 4(c), while d is within the range of the flat section, there is no relative movement between the foot and the footbase. If d moves beyond this range, the foot rolls along the x -axis of the footbase and thus makes relative movement. In this manner, the relative pose of the foot is parameterized by d as $p''(d)$ and $\phi(d)$, where the definition of these functions depend on the selected curve type. See the appendix for concrete definition. For the support foot, d is given

by the x -coordinate of the ZMP expressed in the local coordinate of the footbase; namely,

$$d = [1 \quad 0 \quad 0] R_z(\theta)^T (\mathbf{p}_{\text{zmp}} - \mathbf{p}') \quad (17)$$

In forward walking, the ZMP typically moves from the heel to the toe while the foot is in contact with the ground. Therefore, by parameterizing the foot movement by the x -coordinate of the ZMP, natural heel-to-toe movement can be generated. One major difference between circular and clothoid curves is in the continuity of angular velocity. With circular arcs, the angular velocity of the foot is piecewise constant; the angular velocity jumps discontinuously when the ZMP crosses the boundary between the curved and the flat sections. This discontinuity creates impulsive forces that deteriorate the performance of ground reaction force control. With clothoid arcs, on the other hand, the angular velocity changes continuously.

For the swing foot, the procedure is slightly more complicated, since there is no obvious way to determine d . First, ϕ_k and $\dot{\phi}_k$, the pitch angle and its derivative at the end of the previous support phase, ϕ_{k+1} and $\dot{\phi}_{k+1}$, those at the beginning of the next support phase, are obtained. Next, $\phi(t)$ for an arbitrary time instant $t \in [t_k, t_{k+1}]$ is obtained by polynomial interpolation of 3rd or 5th order. We then obtain d by using the inverse function of $\phi(d)$. Finally, we obtain $\mathbf{p}''(d)$ and $\phi(d)$. In this manner, the continuity of the pitch movement of the foot including the boundary between the support phase and the swing phase is ensured. Moreover, d naturally moves from the toe back to the heel during the swing phase, and consequently, the foot pose smoothly changes from toe-off towards heel-strike. One more benefit of the proposed parametrization is that the maximum height of the foot from the ground can be precisely controlled. That is, the maximum height of the footbase is directly parametrized by h_{lift} , and the lowest part of the foot always touches the x -axis of the footbase. Therefore, there is no danger of having the swing foot too high or too low from the ground because of the heel-to-toe movement.

3.4. Automatic adjustment of foot rotation based on stride

As described in the previous subsection, the pitch angle of the support foot is determined by the position of the ZMP relative to the footbase. One can therefore restrict the range of pitch rotation by setting an appropriate range limit on the ZMP. First, let us define the step length of the s -th step as follows.

$$l_s = [1 \quad 0 \quad 0] R_z(\theta_s)^T (\mathbf{p}_{s+1} - \mathbf{p}_s) \quad (18)$$

Moreover, let $\underline{\phi}_s$ and $\bar{\phi}_s$ be the lower and upper bound on the pitch angle of the support foot of the s -th step. We

parametrize them by the stride l_s as follows.

$$\begin{aligned} \underline{\phi}_s &= -k_{\text{heel}} \max(0, l_{s-1} - l_{\text{flat}}), \\ \bar{\phi}_s &= k_{\text{toe}} \max(0, l_s - l_{\text{flat}}) \end{aligned} \quad (19)$$

Namely, if the stride is smaller than the threshold l_{flat} , the pitch angle is fixed to 0, which results in flat-contact walking. If the stride is greater than l_{flat} , the lower and upper bound are expanded linearly by the rate k_{heel} and k_{toe} , respectively. Given these limits, the corresponding limit on the ZMP can be obtained by using the inverse of $\phi(d)$.

$$\underline{p}_{\text{zmp},x,s} = \phi^{-1}(\underline{\phi}_s), \quad \bar{p}_{\text{zmp},x,s} = \phi^{-1}(\bar{\phi}_s) \quad (20)$$

Here, $\underline{p}_{\text{zmp},x,s}$ and $\bar{p}_{\text{zmp},x,s}$ are the x component of $\mathbf{p}_{\text{zmp},s}$ and $\bar{\mathbf{p}}_{\text{zmp},s}$ that appeared in (11), respectively.

4. Simulation experiment

A block diagram of the whole-body control system used in the simulation experiment is shown in Figure 6. Detailed description is omitted due to the limitation of space. The inverse kinematics solver computes a least-squares problem that is to minimize the tracking error of the reference CoM position and the reference foot pose. An additional cost to penalize angular momentum is included. As a result, arm-swinging motion to cancel angular momentum caused by leg swinging is automatically generated. The reference ZMP and weight ratio of each foot are converted to desired contact wrench and input to the inverse dynamics solver, which outputs desired joint torques. Each joint of the robot is driven by a simple PD controller which accepts desired joint angle and velocity together with desired joint torque. A simple balance feedback is implemented; moment to regulate the angular velocity of the base link is computed by linear feedback, and added to desired contact wrench.

A model of RHP Kaleido, a life-sized humanoid robot developed by Kawasaki Heavy Industry [18] is used for simulation Figure 7(a). The kinematic and inertial parameters of the model are matched to the real robot. A close-up of the foot model with circular arcs is shown in Figure 7(b). For the foot model with circular arcs, parameters are set as $l_{\text{heel}} = l_{\text{toe}} = 0.07$ m, $r_{\text{heel}} = 0.08$ m, and $r_{\text{toe}} = 0.09$ m (see Figure 5 for the definition of parameters), while for the model with clothoid arcs, parameters are set as $l_{\text{heel}} = l_{\text{toe}} = 0.04$ m, $\kappa_{\text{heel}} = \kappa_{\text{toe}} = 180$ rad/m². The profile of soles with circular and clothoid arcs is shown in Figure 7(c). One can see that the difference between these two profiles is very small, despite the fact that the circular sole has a discontinuity in curvature while the clothoid sole does not. Choreonoid 1.8 [19] with the AIST simulator was used

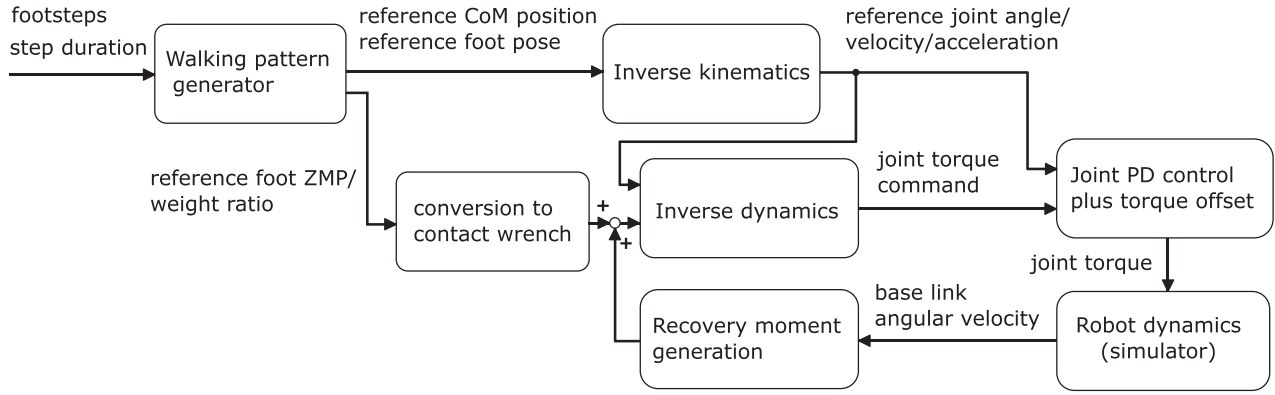


Figure 6. Block diagram of control system.

for simulation. The time step of simulation and the control period were both set as 1 ms. Note that control input computed in each simulation step was input to the simulator in the next simulation step, which means that the controller has a delay of exactly one simulation period (i.e. 1 ms).

An example of generated heel-to-toe walking trajectory with the maximum step length of 0.7 m is shown in Figure 8(a, b). Footsteps input to the planner consists of 12 steps, where the step length is initially 0.3 m and it is increased by 0.1 m at every step until it reached the maximum step length of 0.7 m, and then it is decreased by the same amount until it reached the terminal position. The lateral spacing is set as 0.205 m, which matches the lateral displacement of the hip joints of the robot. The duration of the single support phase and that of the double support phase are set as 0.50 and 0.05 s, respectively. The height of the CoM was set as $h = 0.98$ m and the maximum height of the swing foot from the ground was set as $h_{\text{lift}} = 0.03$ m. The parameters that control the maximum pitch angle are set as $l_{\text{flat}} = 0.3$, $k_{\text{heel}} = 40$ deg/m, $k_{\text{toe}} = 120$ deg/m. In, Figure 8(a), the ZMP of the right and left foot are depicted by red and blue lines, respectively, while the ZMP (i.e. the weighted average of the foot ZMPs) is depicted by the thin black line. The CoM trajectory is depicted by thick black line. A stick plot of whole-body walking movement is shown in Figure 8(b).

Moreover, the pitch angle of each foot is plotted in Figure 9(a–b). Here, Figure 9(a) shows the same walking pattern as Figure 8, while Figure 9(b) shows another walking pattern with the DSP duration set as 0.2 s for comparison. Thanks to the mechanism described in Section 3.4, seamless transition from flat-contact gait to heel-to-contact gait realized. Moreover, the magnitude of pitch rotation increases in accordance with the step length. In close observation, we can see that Figure 9(a,b) shows different transitions of walking gaits. Namely, in Figure 9(a), flat-contact walking directly switches to

heel-to-toe walking where heel-off occurs during SSP. In Figure 9(b), on the other hand, flat-contact walking first switches to a type of heel-to-toe walking where heel-off occurs during DSP, and then it switches to another type where heel-off occurs during SSP. These results demonstrate that the proposed method is able to generate all three walking gaits illustrated in Figure 1 depending on step length and step duration.

The joint angle trajectory of flat-contact walking and heel-to-toe walking with the clothoid foot model are compared. For flat-contact walking, the maximum step length was varied from 200 to 450 mm. Here, l_{flat} was set large enough so that flat-contact walking is enforced. The joint angle trajectories of the hip-pitch, knee, and ankle-pitch joints of the right leg for a single walking cycle are shown in Figure 10(a). It can be seen that the knee joint becomes almost fully stretched near lift-off and landing. Moreover, the first peak of knee stretching comes after lift-off. This implies that the knee must stretch, bend, and stretch again in rapid succession during the swing phase. This is in stark contrast with human walking in which the knee starts to bend before lift-off [2]. Mainly due to this rapid knee movement, with a slightly greater step length such as 470 mm, the knee joint became completely stretched and walking became unstable.

For heel-to-toe walking, the maximum step was varied from 200 to 800 mm. The joint angle trajectories are shown in Figure 10(b). One remarkable difference from flat-contact walking is that knee stretching near lift-off is significantly reduced, thanks to lifting of heel. As a side-effect, the ankle movement during the swing phase is increased, which we consider is acceptable. This is because similar behavior is more or less observed in human walking, and it is harmless compared to knee stretching after lift-off.

Figure 11(a,b) compares how accurately the desired weight ratio and desired ZMP trajectories are tracked in heel-to-toe walking based on different foot models

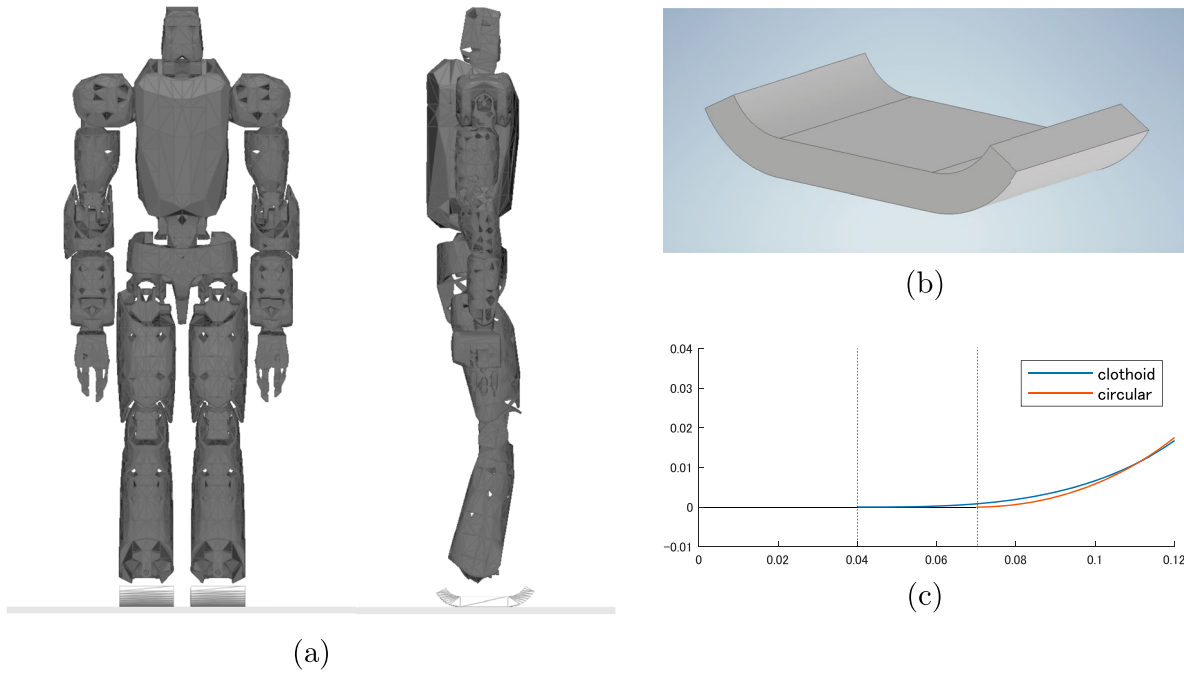


Figure 7. Simulation model of the robot. (a) Model of the humanoid robot Kaleido, (b) a closer view of the foot model and (c) circular and clothoid sole profiles for the front half of the sole (units in m).

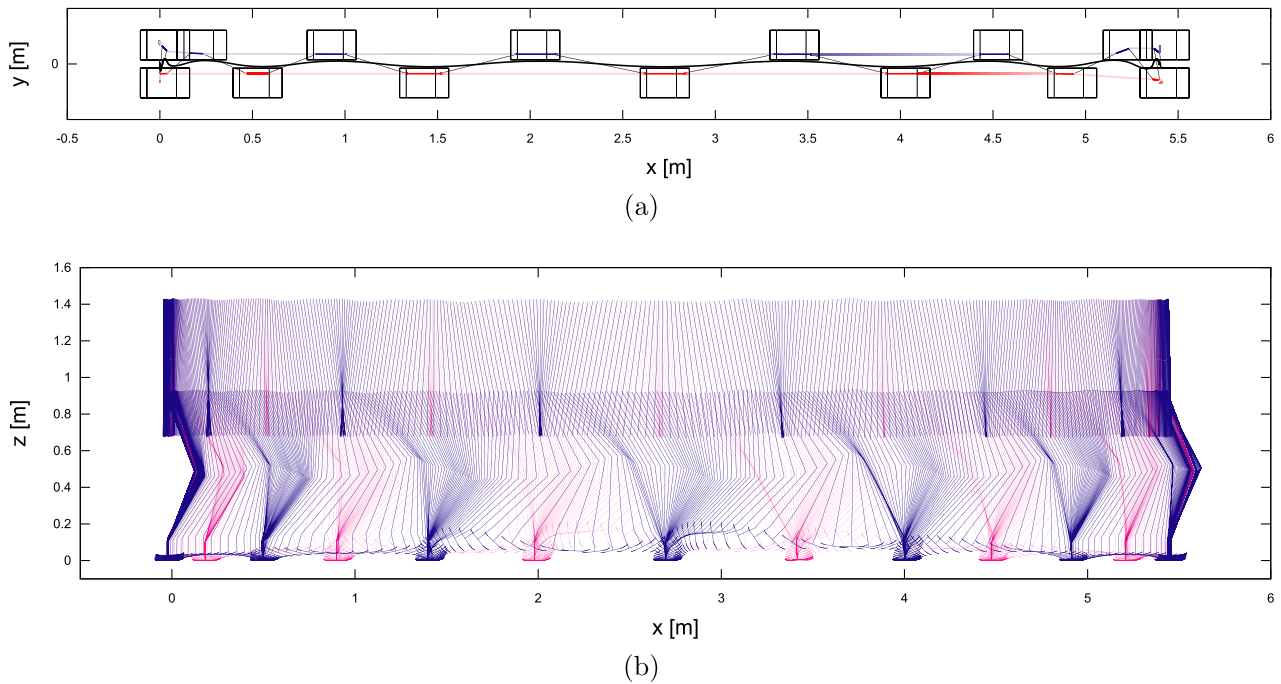


Figure 8. Generated trajectory of heel-to-toe walking with 700 mm maximum step length. (a) CoM and ZMP trajectory and (b) stick plot.

(circular and clothoid). The maximum step length was set to 500 mm. In both settings, the reference weight ratio is tracked with sufficient accuracy, except for double support phases where some fluctuation is observed. A notable difference is seen in the tracking performance of the ZMP. In the case of circular foot, impulsive fluctuation of the ZMP is observed at every transition from

heel-contact to mid-stance. This is because the angular velocity of the foot changes discontinuously at this instant. In the case of clothoid foot, similar phenomenon is still observed but in a much smaller magnitude thanks to the continuity of angular velocity of the foot. From this observation, we conclude that the clothoid foot model is more effective in reducing impulsive forces between the

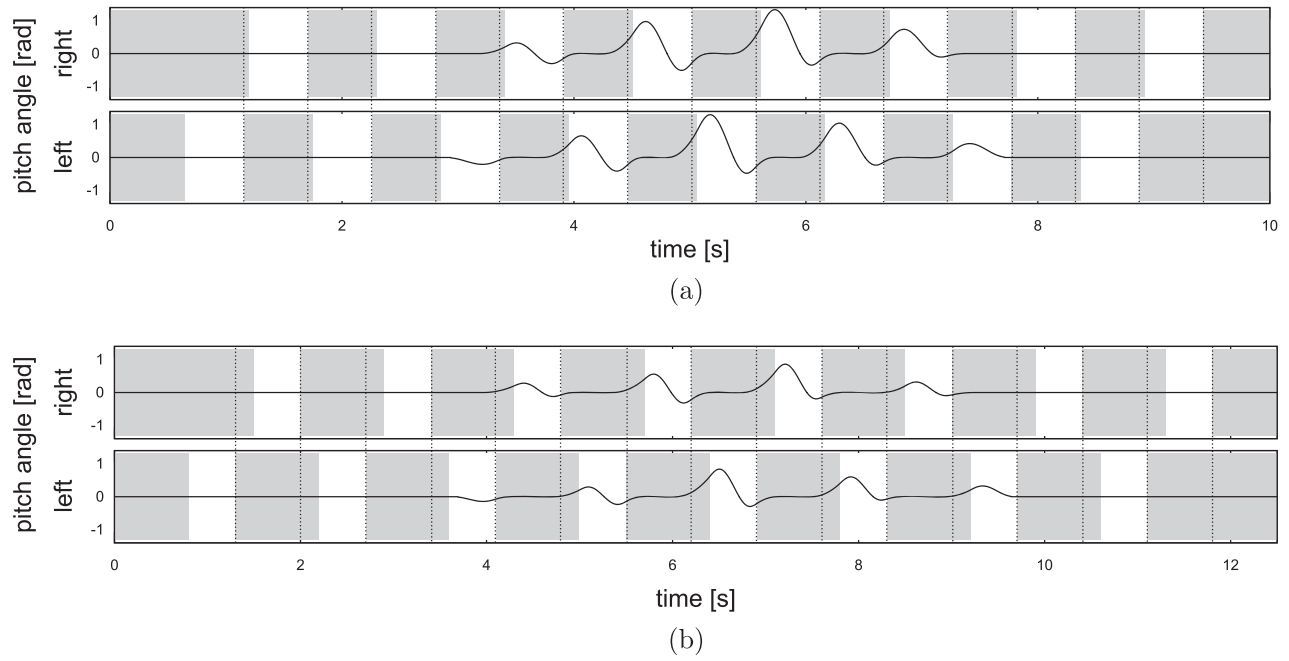


Figure 9. Contact and pitch rotation of feet. Gray background indicates periods in which the foot is in contact with the ground. (a) Maximum step length 700 mm, DSP duration 0.05 s and (b) maximum step length 600 mm, DSP duration 0.2 s.

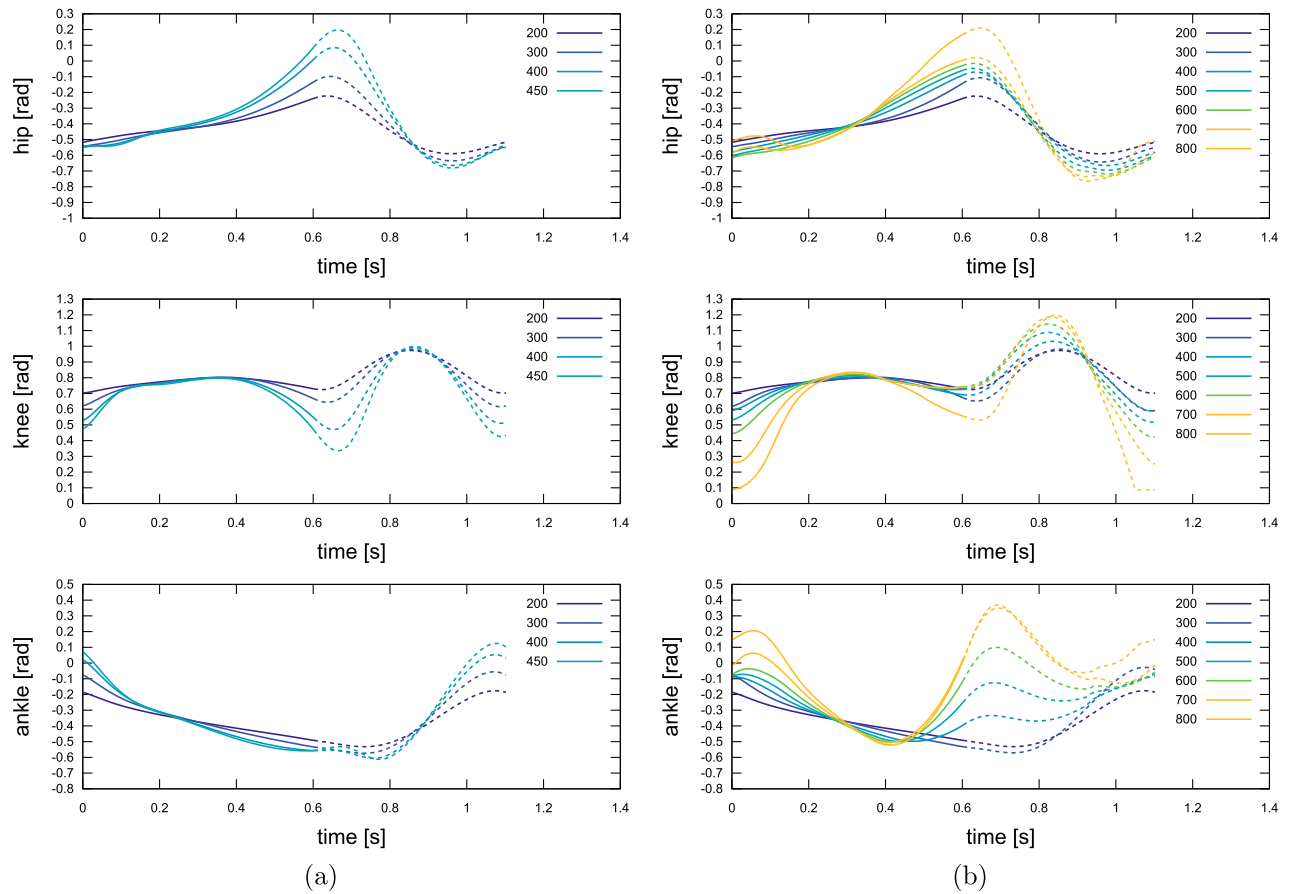


Figure 10. Joint angle trajectories of flat-contact and heel-to-toe walking. Solid and dashed lines indicate the support phase and the swing phase, respectively. (a) Flat-contact and (b) heel-to-toe.

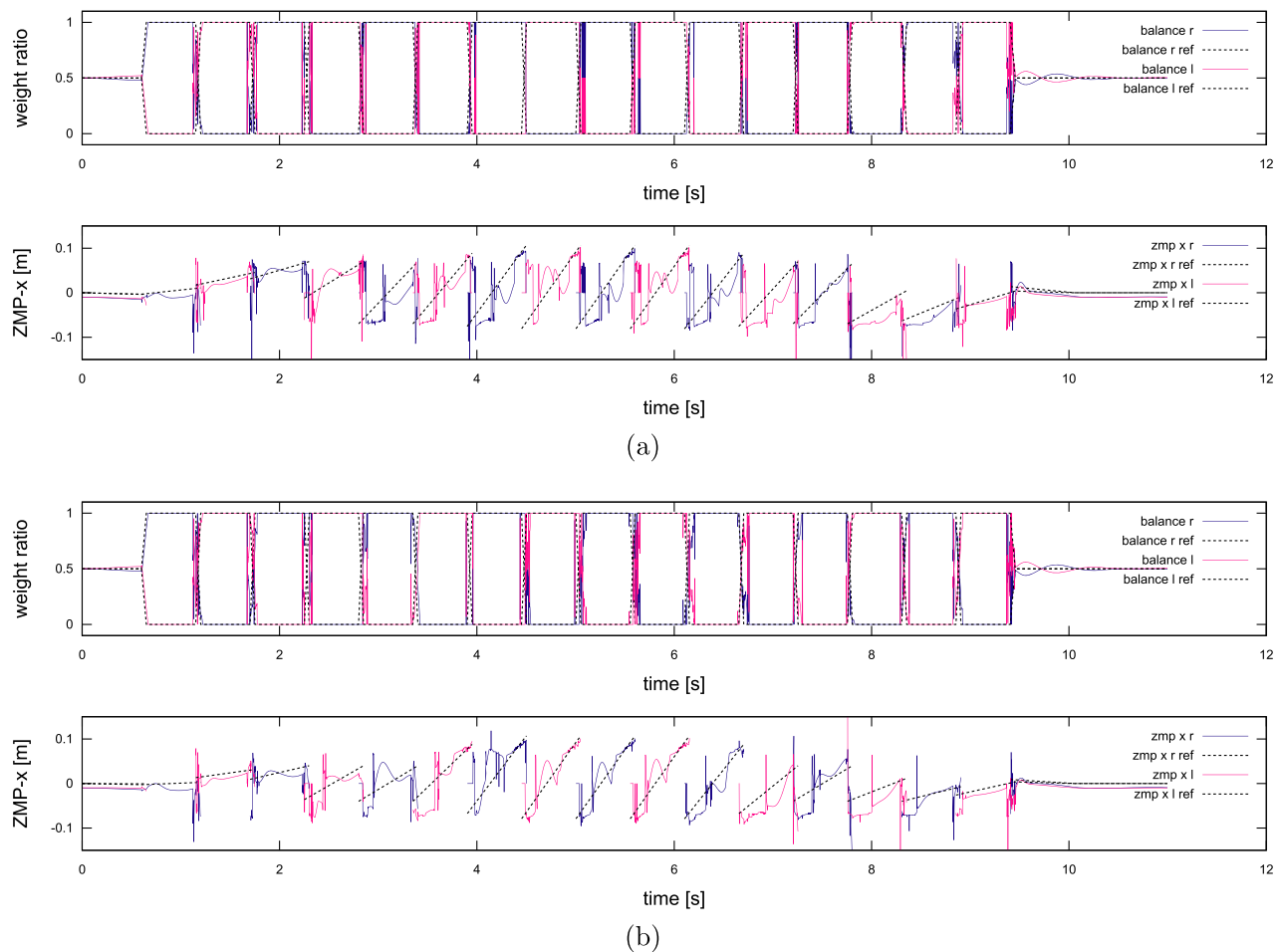


Figure 11. Tracking performance of weight and ZMP. The upper plot of each figure shows the weight ratio between the two feet, while the lower plot shows the x -component of the ZMP of the support foot expressed in the local coordinate of the support foot. For each plot, the reference trajectory generated by the planner is depicted by dashed lines, while the computed physical response is depicted by solid lines. (a) Circular arc foot and (b) clothoid foot.

foot and the ground and achieving better tracking of the reference ZMP.

5. Conclusion

This paper proposed a trajectory generation method for fast and human-like walking of humanoid robots. In simulation, the maximum walking speed of 4.6 km/h was achieved using a model of a life-sized humanoid robot. Our future work includes testing the presented method on a real humanoid robot and extending it to biped running involving toe-off and heel-strike.

Disclosure statement

No potential conflict of interest was reported by the author(s).

Notes on contributors

Yuichi Tazaki received the Dr Eng degree in control engineering from the Tokyo Institute of Technology, Tokyo, Japan, in 2008. From 2007 to 2009, he was a research fellow of the Japan Society for the Promotion of Science. In 2008, he was a guest scientist at Honda Research Institute Europe, Germany. Since 2009 to 2016, he was an assistant professor at Nagoya University, Japan. From 2016, he has been an associate professor at Kobe University, Japan. His research interests include autonomous vehicles, mobile robots, and humanoid robots. He is a member of IEEE, the Society of Instrument and Control Engineers (SICE), and The Robotics Society of Japan.

Satomi Hanasaki received a BS degree in engineering from Kobe University in 2021. He is currently an MS student in the Graduate School of Engineering, Kobe University. His research theme is walking and running trajectory generation for humanoid robots.

Soh Yukizaki received the BS and MS in Information Science and Technology from The University of Tokyo in 2014 and 2017, respectively. Since 2017, he is currently a robotics

software engineer at Kawasaki Heavy Industries, Ltd. His research interests include humanoid robots, control of robots and software for robotics.

Yugo Mitazono is currently a robotics software engineer in Kawasaki Heavy Industries, Ltd. from 2019. His research interests include humanoid robots, control of robots and software for robotics.

Hikaru Nagano received the BS, MS, and PhD degrees in engineering from Nagoya University in 2010, 2012, and 2015, respectively. From 2013 to 2015, he was a research fellow of the Japan Society for the Promotion of Science. From 2015 to 2018, he was an assistant professor at Tohoku University. He is currently an assistant professor in the Department of Mechanical Engineering, Graduate School of Engineering, Kobe University. His research interests include human-machine interfaces and haptic perception.

Yasuyoshi Yokokohji received the BS and MS degrees in Precision Engineering in 1984 and 1986, respectively, and PhD degree in Mechanical Engineering in 1991, all from Kyoto University. From 1988 to 1989, he was a research associate in the Automation Research Laboratory, Kyoto University. From 1989 to 1992, he was a research associate in the Division of Applied Systems Science, Faculty of Engineering, Kyoto University. From 1992 to 2005, he was an associate professor in the Department of Mechanical Engineering, Kyoto University. From 2005 to 2009, he was an associate professor in the Department of Mechanical Engineering and Science, Graduate School of Engineering, Kyoto University. From 1994 to 1996, he was a visiting research scholar at the Robotics Institute, Carnegie Mellon University. Since 2009, he has been a professor in the Department of Mechanical Engineering, Graduate School of Engineering, Kobe University. His current research interests are robotics and virtual reality including teleoperation systems, robot hands, and haptic interfaces. He is a fellow of the Robotics Society of Japan, the Japan Society of Mechanical Engineers, and the Society of Instrument and Control Engineers (Japan), and a member of the Institute of Systems, Control and Information Engineers (Japan), the Virtual Reality Society of Japan, and the IEEE (Senior Member).

ORCID

Yasuyoshi Yokokohji  <http://orcid.org/0000-0001-8869-7102>

References

- [1] Ogura Y, Shimomura K, Kondo H. Human-like walking with knee stretched, heel-contact and toe-off motion by a humanoid robot. *IEEE/RSJ Int. Conf. Intelligent Robots and Systems*; 2006.
- [2] Miura et al K. Human-like walking with toe supporting for humanoids. *IEEE/RSJ International Conference on Intelligent Robots and Systems*; 2011. p. 4428–4435.
- [3] Hurst J. Walk this way: to be useful around people, robots need to learn how to move like we do. *IEEE Spectr.* 2019;56(3):30–51.
- [4] Tajima R, Honda D, Suga K. Fast running experiments involving a humanoid robot. *IEEE International Conference on Robotics and Automation*; 2009. p. 1571–1576.
- [5] Takenaka T, Matsumoto T, Yoshiike T, et al. Real time motion generation and control for biped robot – 2nd report: running gait pattern generation. *IEEE/RSJ International Conference on Intelligent Robots and Systems*; 2009. p. 1092–1099.
- [6] Huang Q, Yokoi K, Kajita S, et al. Planning walking patterns for a biped robot. *IEEE Trans Rob Autom.* 2001;17:280–289.
- [7] Yamamoto K, Sugihara T, Nakamura Y. Gait planning including toe contact with boundary condition relaxation. *The 17th CISM-IFTOMM Symposium (RoManSy17)*; 2008. p. 409–416.
- [8] Erbatur K, Kurt O. Natural ZMP trajectories for biped robot reference generation. *IEEE Trans Ind Electron.* 2009;56(3):835–845.
- [9] Li Z, Vanderborght B, Tsagarakis NG, et al. Fast bipedal walking using large strides by modulating hip posture and toe-heel motion. *International Conference on Robotics and Biomimetics*; 2010. p. 13–18.
- [10] Yi S-J, Lee DD. Dynamic heel-strike toe-off walking controller for full-size modular humanoid robots. *IEEE-RAS 16th International Conference on Humanoid Robots (Humanoids)*; 2016. p. 395–400.
- [11] Chen X, Yu Z, Zhang W, et al. Bio-inspired control of walking with toe-off, heel-strike and disturbance rejection for a biped robot. *IEEE Trans Ind Electron.* 2017;64:7962–7971.
- [12] Shiguematsu YM, Kryczka P, Hashimoto K, et al. Heel-Contact toe-Off walking pattern generator based on the linear inverted pendulum. *Int J Humanoid Robot.* 2016;13(1):1650002.
- [13] Huang Z, Yu Z, Chen X, et al. Knee-Stretched walking with toe-Off and heel-Strike for a position-Controlled humanoid robot based on model predictive control. *Int J Adv Robot Syst.* 2021;18(4):172988142111036282.
- [14] Tanaka K, Sugihara T. Dynamically consistent motion design of a humanoid robot even at the limit of kinematics. *IEEE-RAS International Conference on Humanoid Robots*; 2014. p. 1007–1012.
- [15] Kajita S, Kanehiro F, Kaneko K. Biped walking pattern generation by using preview control of zero-moment point. *IEEE International Conference on Robotics and Automation*; 2003. p. 1620–1626.
- [16] Ezati M, Khadiv M, Moosavian S. Effects of toe-off and heel-off motions on gait performance of biped robots. *RSI Int. Conf. Robotics and Mechatronics*; 2015.
- [17] Sugihara T, Imanishi K, Yamamoto T, et al. 3D biped locomotion control including seamless transition between walking and running via 3D ZMP manipulation. *IEEE International Conference on Robotics and Automation*; 2021. p. 6258–6263.
- [18] Kakiuchi Y, Kamon M, Shimomura N. Development of life-sized humanoid robot platform with robustness for falling down, long time working and error occurrence. *IEEE/RSJ International Conference on Intelligent Robots and Systems*; 2017. p. 689–696.
- [19] Choreonoid homepage. Available from: <https://choreonoid.org/>

Appendix

In the following, the parametrization of the relative movement of the foot with respect to the footbase is described in detail. For simplicity of notation, the foot label i is omitted. Let $\tilde{\mathbf{p}}(d)$ denote the position of the contact point expressed in the local coordinate of the foot. Given $\tilde{\mathbf{p}}(d)$ and $\phi(d)$, the position of the foot \mathbf{p}'' in the local coordinate of the footbase is given by

$$\mathbf{p}''(d) = \begin{bmatrix} d \\ 0 \end{bmatrix} - R(-\phi(d))\tilde{\mathbf{p}}(d)$$

The definition of $\tilde{\mathbf{p}}(d)$ and $\phi(d)$ differs depending on the type of the heel and toe curves. If the curves are circular, we have

$$\begin{cases} \phi(d) = \frac{d + l_{\text{heel}}}{r_{\text{heel}}}, \\ \tilde{\mathbf{p}}(d) = \begin{bmatrix} -l_{\text{heel}} + r_{\text{heel}} \sin \phi(d) \\ r_{\text{heel}}(1 - \cos \phi(d)) \end{bmatrix} & \text{if } d < -l_{\text{heel}} \\ \phi(d) = \frac{d - l_{\text{toe}}}{r_{\text{toe}}}, \\ \tilde{\mathbf{p}}(d) = \begin{bmatrix} l_{\text{toe}} + r_{\text{toe}} \sin \phi(d) \\ r_{\text{toe}}(1 - \cos \phi(d)) \end{bmatrix} & \text{if } d > l_{\text{toe}} \\ \phi(d) = 0, \\ \tilde{\mathbf{p}}(d) = 0 & \text{otherwise} \end{cases} \quad (\text{A1})$$

where r_{heel} and r_{toe} are the radius of the heel arc and the toe arc, respectively.

If the curves are clothoid, we have

$$\begin{cases} \phi(d) = -\frac{1}{2}\kappa_{\text{heel}}(d + l_{\text{heel}})^2, \\ \tilde{\mathbf{p}}(d) = \begin{bmatrix} -l_{\text{heel}} - \sqrt{\frac{2}{\kappa_{\text{heel}}}} C\left(-\sqrt{\frac{\kappa_{\text{heel}}}{2}}(d + l_{\text{heel}})\right) \\ \sqrt{\frac{2}{\kappa_{\text{heel}}}} S\left(-\sqrt{\frac{\kappa_{\text{heel}}}{2}}(d + l_{\text{heel}})\right) \end{bmatrix} & \text{if } d < -l_{\text{heel}} \\ \phi(d) = \frac{1}{2}\kappa_{\text{toe}}(d - l_{\text{toe}})^2, \\ \tilde{\mathbf{p}}(d) = \begin{bmatrix} l_{\text{toe}} + \sqrt{\frac{2}{\kappa_{\text{toe}}}} C\left(\sqrt{\frac{\kappa_{\text{toe}}}{2}}(d - l_{\text{toe}})\right) \\ \sqrt{\frac{2}{\kappa_{\text{toe}}}} S\left(\sqrt{\frac{\kappa_{\text{toe}}}{2}}(d - l_{\text{toe}})\right) \end{bmatrix} & \text{if } d > l_{\text{toe}} \\ \phi(d) = 0, \\ \tilde{\mathbf{p}}(d) = 0 & \text{otherwise} \end{cases} \quad (\text{A2})$$

where κ_{heel} and κ_{toe} are the rate of change of curvature of the heel arc and the toe arc, respectively. Moreover, $C(s)$ and $S(s)$ are the Fresnel integrals defined as

$$C(s) = \int_0^s \cos(t^2) dt, \quad S(s) = \int_0^s \sin(t^2) dt.$$

The power series expansion of the Fresnel integrals is used to compute their approximate values.